



Universiteit
Leiden
The Netherlands

Electrochemical and surface studies of the effect of naphthalene-based additives on tin electrodeposition

Aranzales Ochoa, D.M.

Citation

Aranzales Ochoa, D. M. (2021, March 17). *Electrochemical and surface studies of the effect of naphthalene-based additives on tin electrodeposition*. Retrieved from <https://hdl.handle.net/1887/3151629>

Version: Publisher's Version

License: [Licence agreement concerning inclusion of doctoral thesis in the Institutional Repository of the University of Leiden](#)

Downloaded from: <https://hdl.handle.net/1887/3151629>

Note: To cite this publication please use the final published version (if applicable).

Cover Page



Universiteit Leiden



The handle <http://hdl.handle.net/1887/3151629> holds various files of this Leiden University dissertation.

Author: Aranzales Ochoa, D.M.

Title: Electrochemical and surface studies of the effect of naphthalene-based additives on tin electrodeposition

Issue date: 2021-03-17

Appendices

APPENDIX

A

Supporting information to Chapter 2:

Voltammetric study of tin
electrodeposition on polycrystalline gold
from sulfuric and methanesulfonic acid

A.1 Cluster formation during underpotential (UPD) and overpotential (OPD) tin deposition

Fig. A1 shows SEM images of nano-clusters formed in the early stages of the deposition (UPD), their growth and subsequent coalescence in the following stages (OPD).

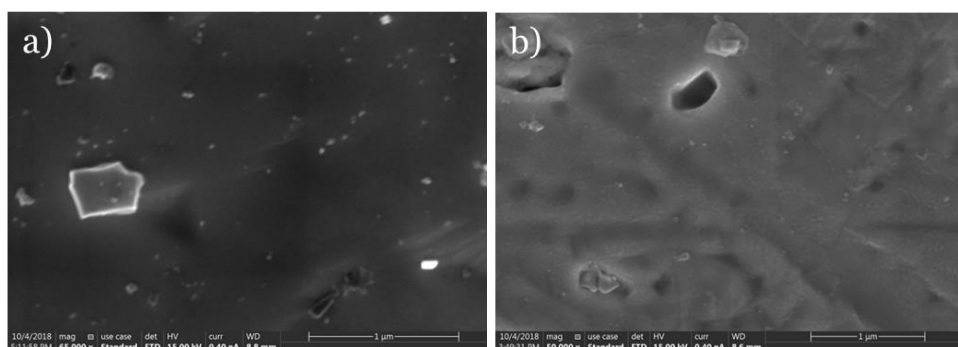


Figure A1. SEM images potentiostatic deposition of tin on polycrystalline gold electrodes in SA. a) Underpotential deposition (-0.1 V vs. RHE during 1 min). b) Overpotential deposition (-0.2 V vs. RHE during 1 min)

A.2 Concurrent HER during overpotential tin deposition

Figures A2 and A3 show that at 30 mV s^{-1} the current-voltage curves are not completely sigmoidal, and the plateau current does not vary linearly with the square root of the rotation rate in the Koutecky-Levich plots (inset), which indicates that under the present conditions no fully diffusion-limited current values are reached, neither in SA nor in MSA. This unusual behavior is related to a concurrent HER on the gold surface during the deposition process, which is likely to be present due to cluster formation, where a partial coverage of the surface is exhibited.

A.3 Limiting diffusion control reached at low scan rates

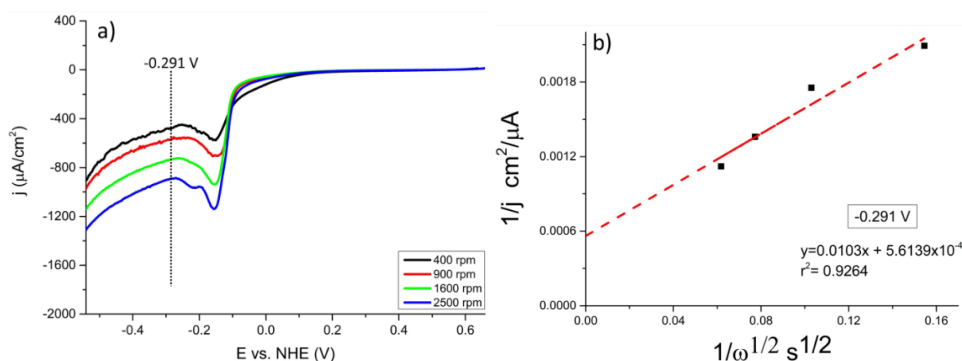


Figure A2. a) Linear sweep voltammograms of tin deposition from sulfuric acid on a gold rotating disc electrode. Concentration of solution Sn^{2+} 0.6 mM. Scan rate 30 mV s^{-1} ; rotation rate 400, 900, 1600 and 2500 rpm. b) Koutecky-Levich plot.

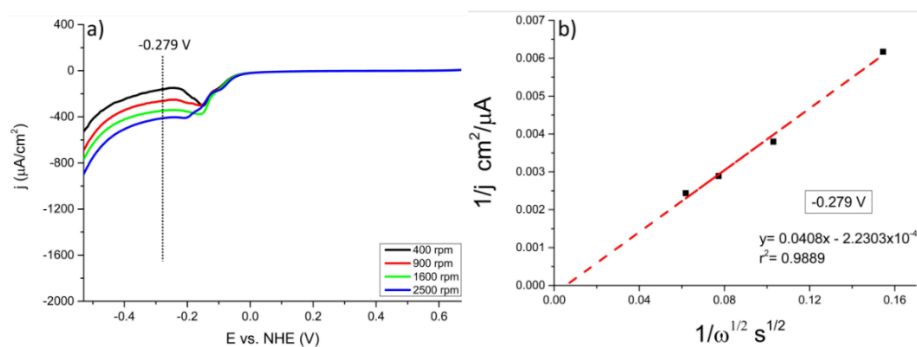


Figure A3. a) Linear sweep voltammograms of tin deposition from methanesulfonic acid on a gold rotating disc electrode. Concentration of solution Sn^{2+} 0.6 mM. Scan rate 30 mV s^{-1} ; rotation rate 400, 900, 1600 and 2500 rpm. b) Koutecky-Levich plot.

A.3 Limiting diffusion control reached at low scan rates

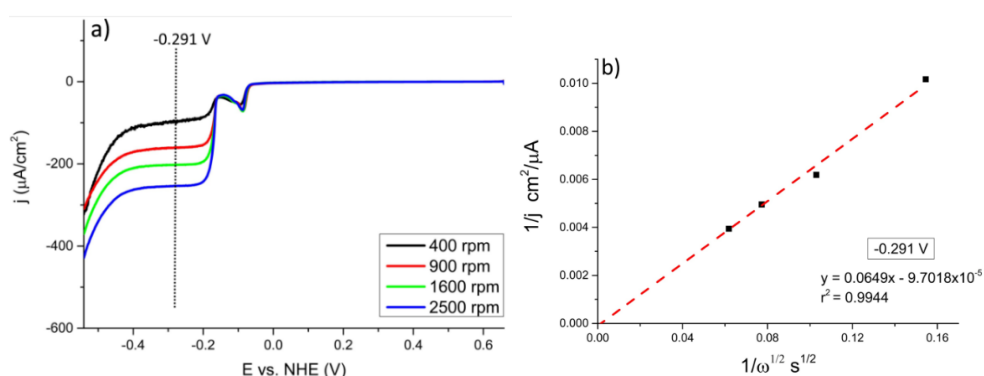


Figure A4. a) Linear sweep voltammograms of tin deposition from sulfuric acid on a gold rotating disc electrode. Concentration of solution Sn^{2+} 0.6 mM. Scan rate 2 mV s^{-1} ; rotation rate 400, 900, 1600 and 2500 rpm. b) Koutecky-Levich plot.

Appendix A: Supporting information to Chapter 2

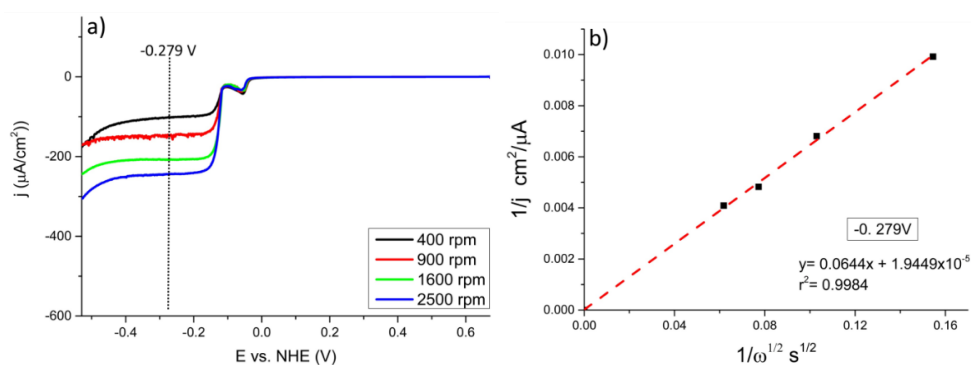


Figure A5. a) Linear sweep voltammograms of tin deposition from methanesulfonic acid on a gold rotating disc electrode. Concentration of solution Sn^{2+} 0.6 mM. Scan rate 2 mV s^{-1} ; rotation rate 400, 900, 1600 and 2500 rpm. b) Koutecky-Levich plot.

As it has been already mentioned in the chapter, low scan rate leads to more tin deposition and subsequently a complete coverage of the gold surface, avoiding any concurrent non-desirable side reaction, such as HER on gold. A full mass transport control region is seen in SA and MSA, following the Koutecky-Levich behavior.

APPENDIX

B

Supporting information to Chapter 3:

The effect of naphthalene-based additives
on tin electrodeposition on a gold
electrode

B.1 Concentration effect of NPT, NPTS, HNPTS and ENSA on the gold surface

Figures B1, B2 and B3 show the cyclic voltammograms of NPT, NPTS, HNPTS and ENSA at different concentrations on gold single crystal surfaces.

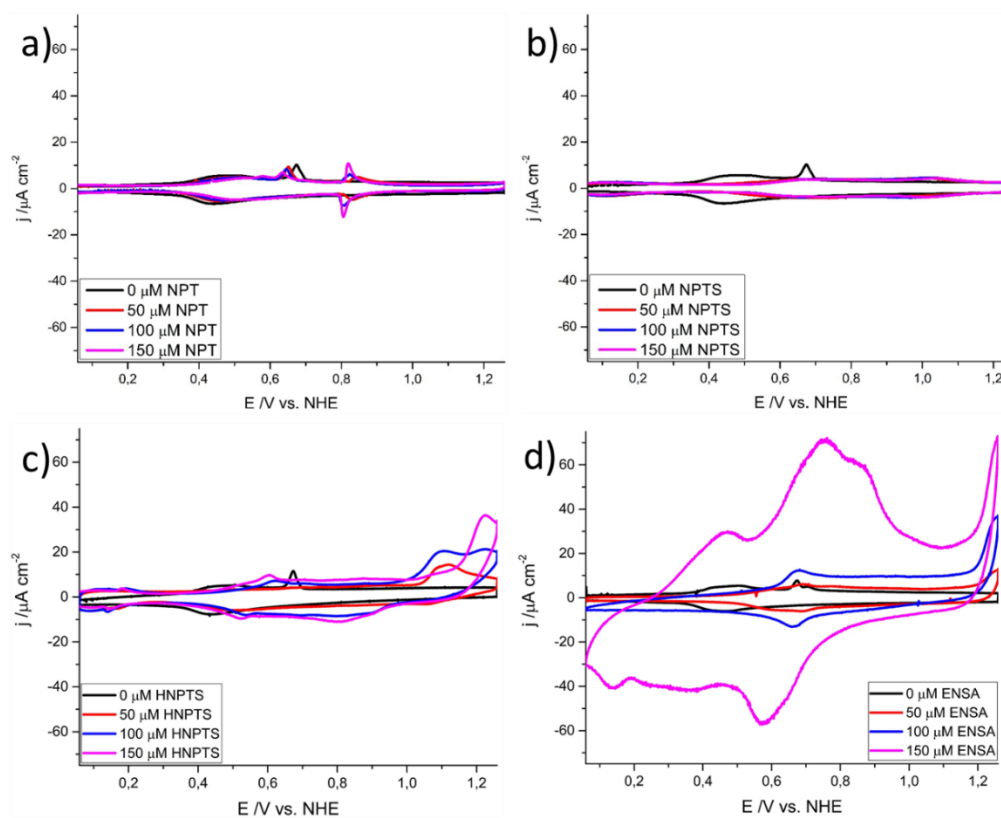


Fig B1. Cyclic voltammograms of Au (100), 0.1 M H₂SO₄ at different concentrations of (a) NPT (b) NPTS (c) HNPTS (d) ENSA recorded between 0,06 to 1.26 V DL- region, at 50 mV s⁻¹.

B.1 Concentration effect of NPT, NPTS, HNPTS and ENSA on the gold surface

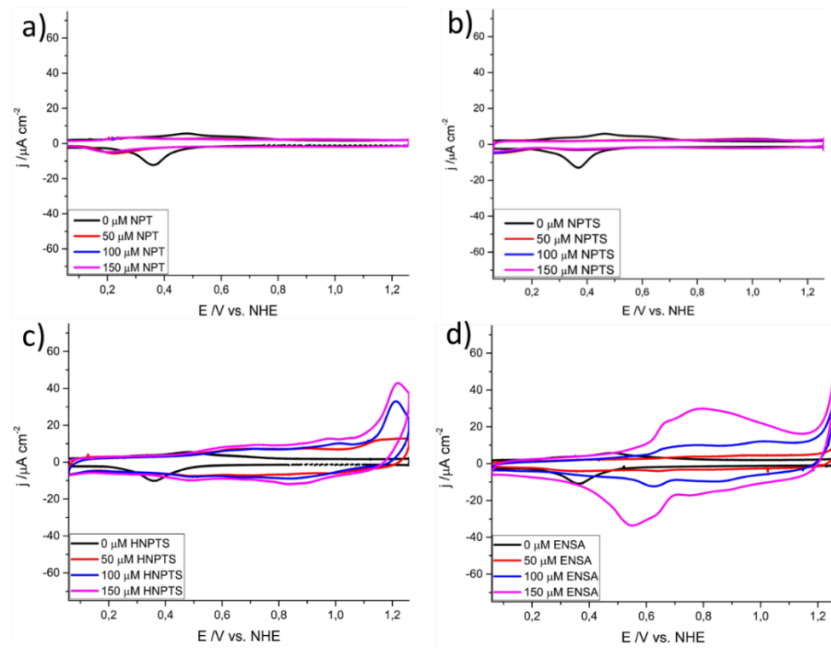


Fig B2. Cyclic voltammograms of Au (110), 0.1 M H_2SO_4 at different concentrations (a) NPT (b) NPTS (c) HNPTS (d) ENSA recorded between 0,06 to 1.26 V DL- region, at 50 mV s^{-1} .

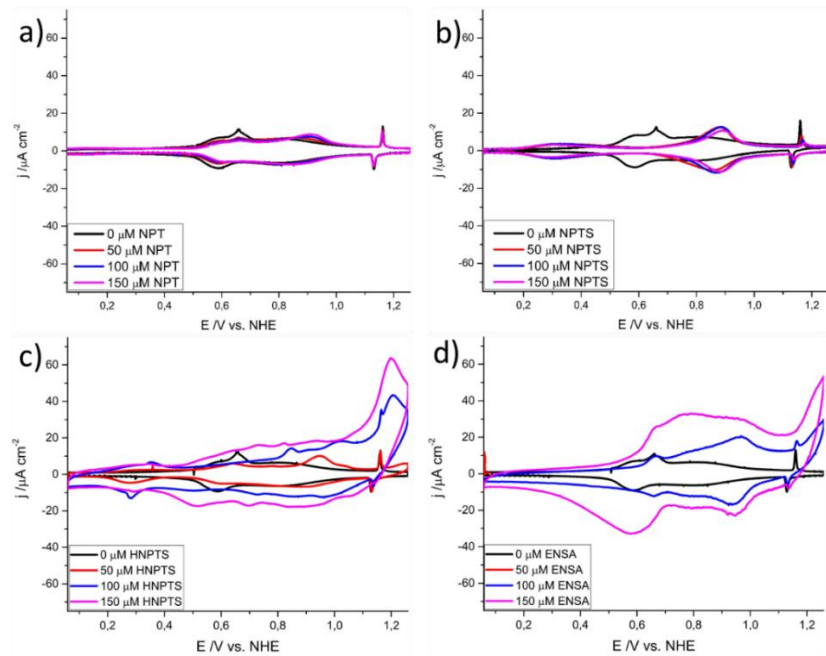


Fig B3. Cyclic voltammograms of Au (111), 0.1 M H_2SO_4 at different concentrations of ((a) NPT (b) NPTS (c) HNPTS (d) ENSA recorded between 0,06 to 1.26 V DL- region, at 50 mV s^{-1} .

B.2 Delay in the phase transition of sulfate adlayer as a consequence of NPT adsorption

Fig B4. shows the characteristic voltammogram of the double layer region of Au (100) in HClO₄ electrolyte^{1, 2} (black line). When NPT is added (red line) a decrease in the capacitive current is observed, which is characteristic of 2D film formation. However, no sharp peak at about 0.81 V is seen, in contrast to what is observed in H₂SO₄ (Fig. B1 a). After the sulfate addition two reversible couples of peaks appear. The first couple at about 0.75 V is ascribed to sulfate specific adsorption and the second at 1.05 V to disorder – order transition in the sulfate adlayer. The peaks also shift slightly towards lower potentials with the higher sulfate concentration, as expected.

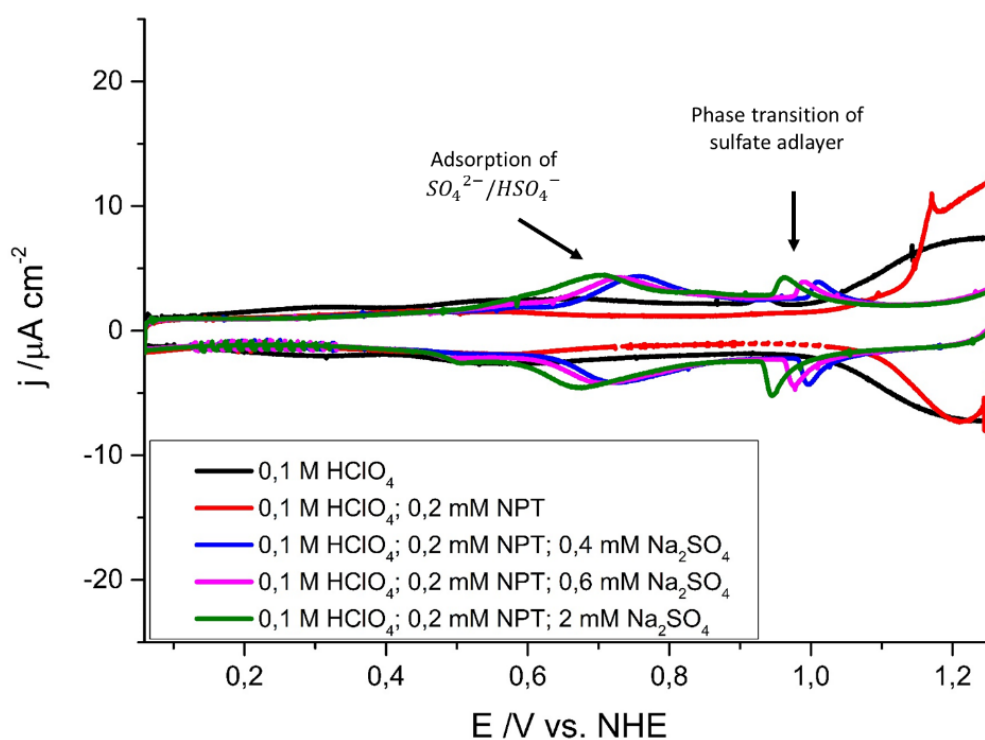


Fig B4. Cyclic voltammograms of Au (100), 0.1 M HClO₄, 0.2 mM NPT at different Na₂SO₄ concentrations. Recorded between 0.06 to 1.26 V DL- region

B.3 Naphthalene (NPT), naphthalenesulfonate (NPTS), hydroxynaphthalene sulfonic acid (HNPTS) and α -ethoxylated naphthalene sulfonic acid (ENSA) adsorption on the gold surface

The linear relationship between the peak current (I_p) and the scan rate (ν) is used as an argument to assign the peaks to processes related to adsorbed species. Figures B5, B6, and B7 show the mentioned linear relationship for some of the peaks of NPT, NPTS and HNPTS, but not for ENSA on the Au single crystals surfaces, which agrees with the oxidative polymerization process.

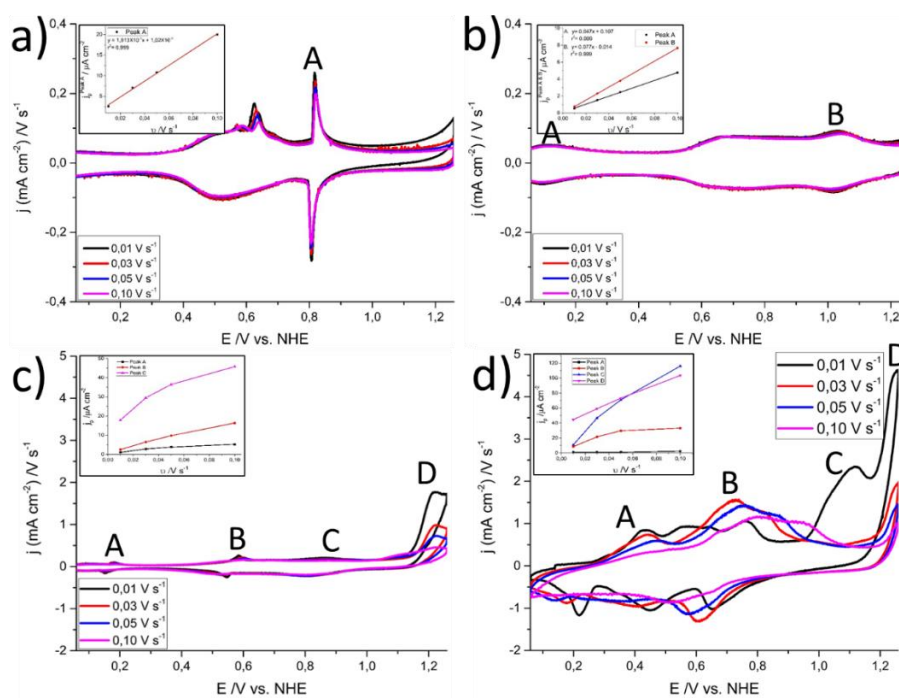


Fig B5. Cyclic voltammograms of Au (100), 0.1 M H₂SO₄ (a) 150 μ M NPT and (b) 150 μ M NPTS (c) 150 μ M HNPTS (d) 150 μ M ENSA recorded between 0,06 to 1.26 V DL- region, at different scan rates.

Appendix B: Supporting information to Chapter 3

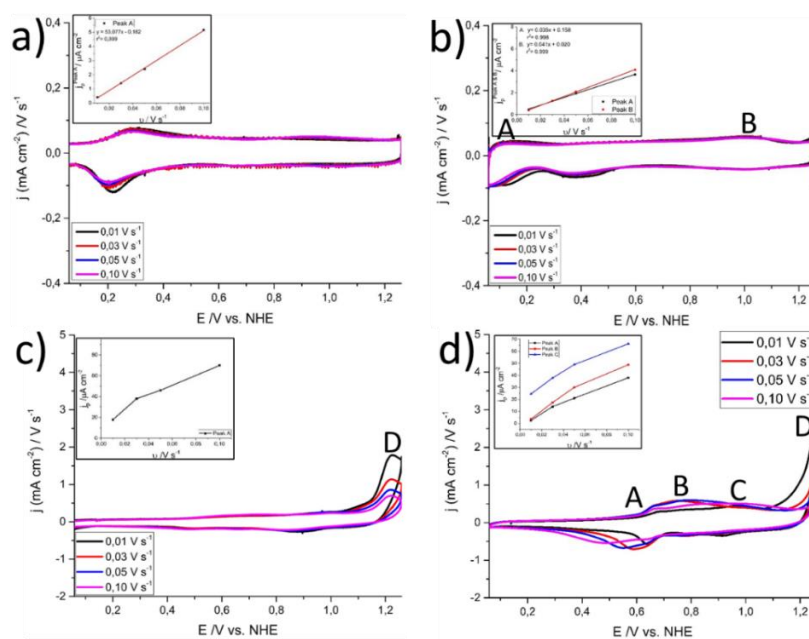


Fig B6. Cyclic voltammograms of Au (110), 0.1 M H₂SO₄ (a) 150 μM NPT and (b) 150 μM NPTS (c) 150 μM HNPTS (d) 150 μM ENSA recorded between 0,06 to 1.26 V DL- region, at different scan rates.

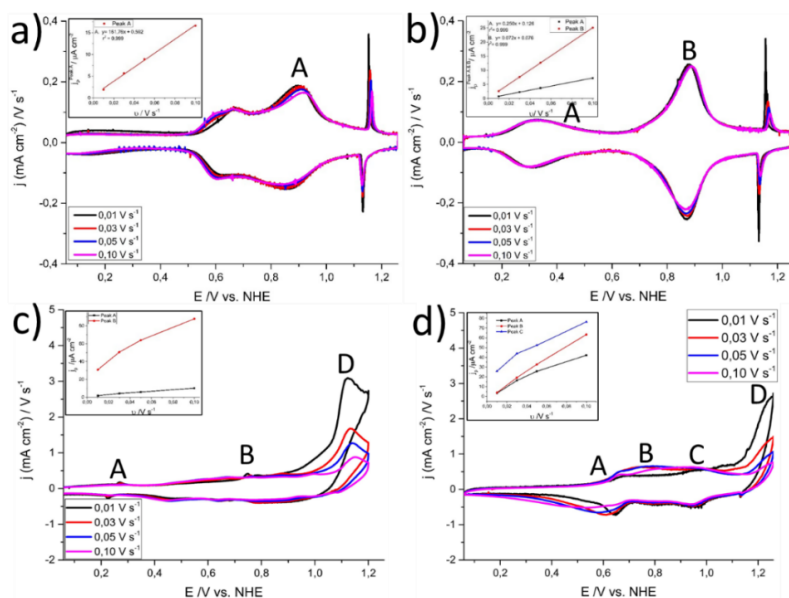


Fig B7. Cyclic voltammograms of Au (111), 0.1 M H₂SO₄ (a) 150 μM NPT and (b) 150 μM NPTS (c) 150 μM HNPTS (d) 150 μM ENSA recorded between 0,06 to 1.26 V DL- region, at different scan rates.

B.4 Surface enhanced Raman spectroscopy of NPT, NPTS, HNPTS and ENSA on the gold surface

Fig. B8, B9, B10 and B11 show the evolution of SER spectra of NPT, NPTS, HNPTS and ENSA on roughened gold electrode, recorded between 0.01 to 1.06 V.

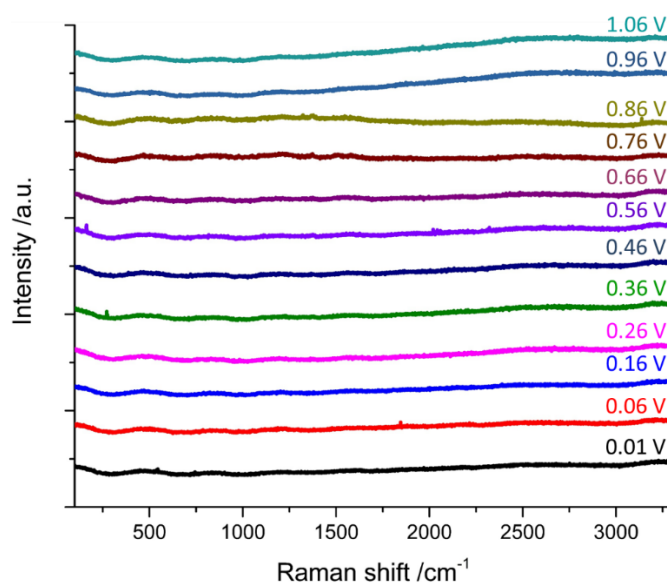


Figure B8. SER spectrum of 0.2 mM of NPT in 0.1 M H_2SO_4 on polycrystalline gold at different potentials from 0.01 to 1.06 V

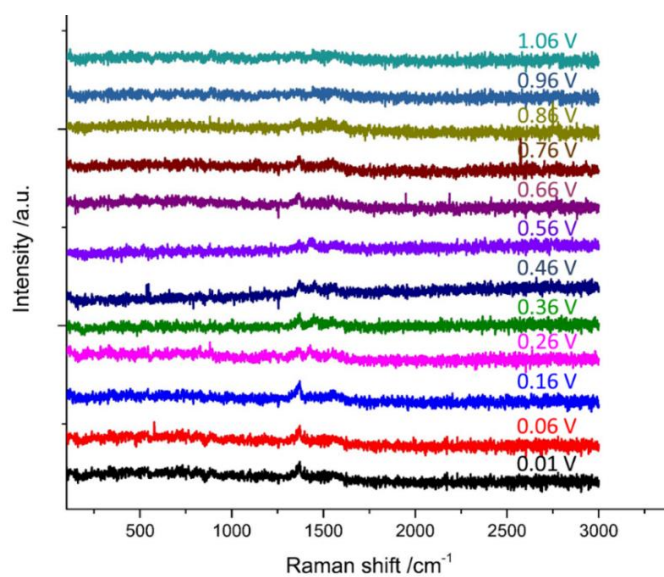


Figure B9. SER spectrum of 1 mM of NPTS in 0.1 M H_2SO_4 on polycrystalline gold at different potentials from 0.01 to 1.06 V

Appendix B: Supporting information to Chapter 3

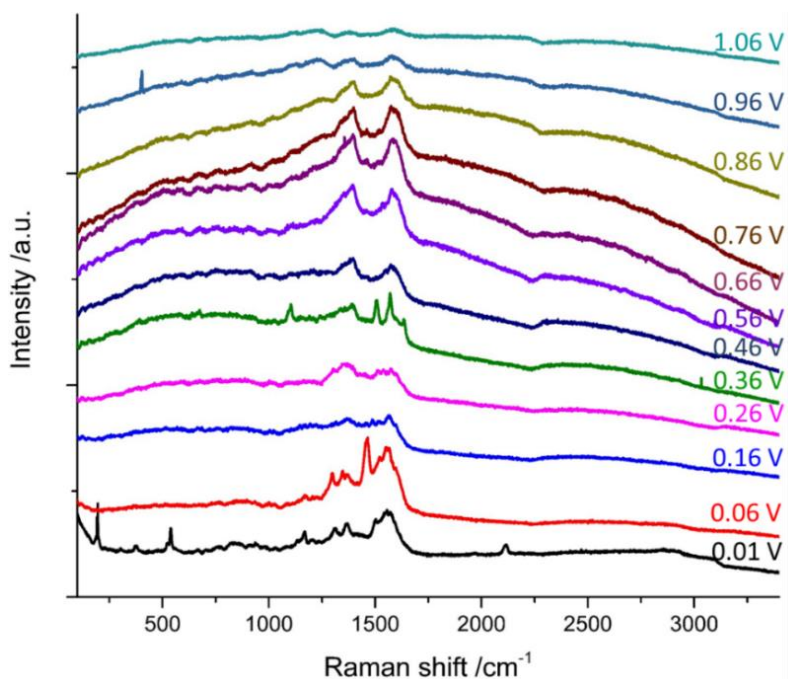


Figure B10. SER spectrum of 1 mM of HNPTS in 0.1 M H_2SO_4 on polycrystalline gold at different potentials from 0.01 to 1.06 V

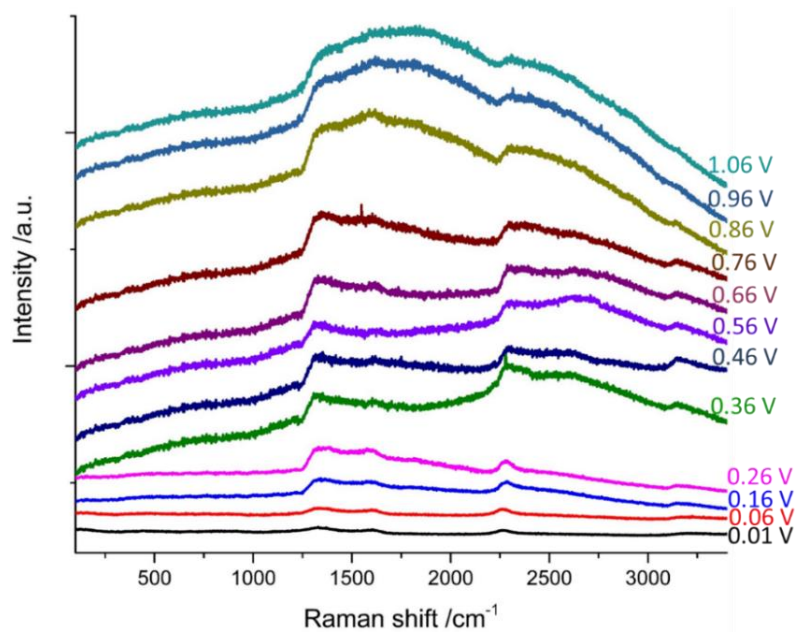


Figure B11. SER spectrum of 1 mM of ENSA in 0.1 M H_2SO_4 on polycrystalline gold at different potentials from 0.01 to 1.06 V

B.5 Density functional theory study

Figure B12 shows the calculation of the lateral interaction energy between NPT and NPTS molecules, with the configuration which exhibits the highest possible attractive interaction on Au (111).

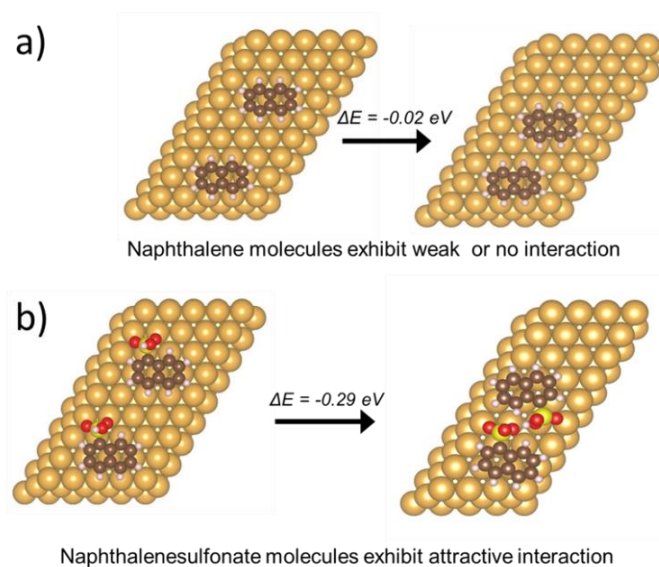


Fig B12. Difference of lateral interaction energy between (a) naphthalene and (b) naphthalenesulfonate

Figures B13 and B14 show the calculation of the lateral interaction energy between NPT and NPTS molecules, with the configuration which exhibits the highest possible attractive interaction on Sn (111).

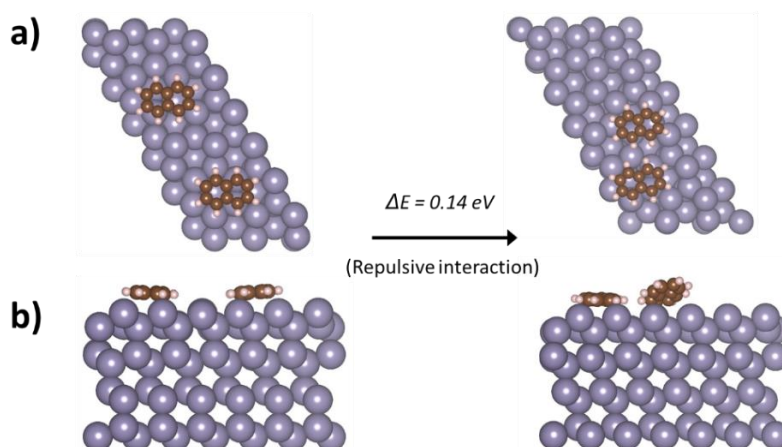


Fig B13. Difference of lateral interaction energy between naphthalene (a) top-down view and (b) lateral view

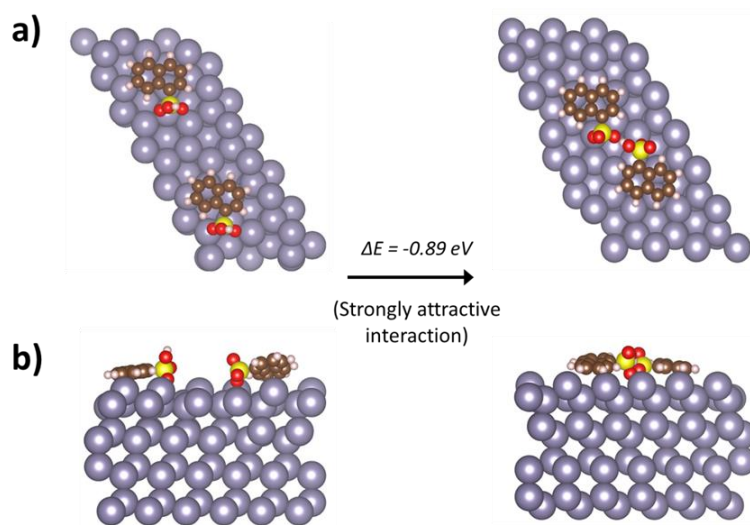


Fig B14. Difference of lateral interaction energy between naphthalenesulfonate (a) top-down view and (b) lateral view

B.6 Shift of the peak A2 is not kinetic in nature

Figure B15 shows the measurements of the scan rate dependence in the presence of naphthalenesulfonate. It is observed that peak A2 is not affected by the scan rate. Peak positions stay almost at the same potential, showing that the phenomenon is not related to a kinetic effect (or to diffusion from the bulk to the surface), instead is related to the thermodynamics of the process, a change in the composition of the Au-Sn alloy is likely.

Inset of the Fig. B15 shows the EDX spectrum for a nanoparticle of the tin deposit, showing small amounts of oxygen and sulfur in the deposit. Oxygen is not a surprise; it must be incorporated during the transfer to the SEM equipment due to the oxidative nature of tin.

B.7 Number of Sn ML on the gold substrate

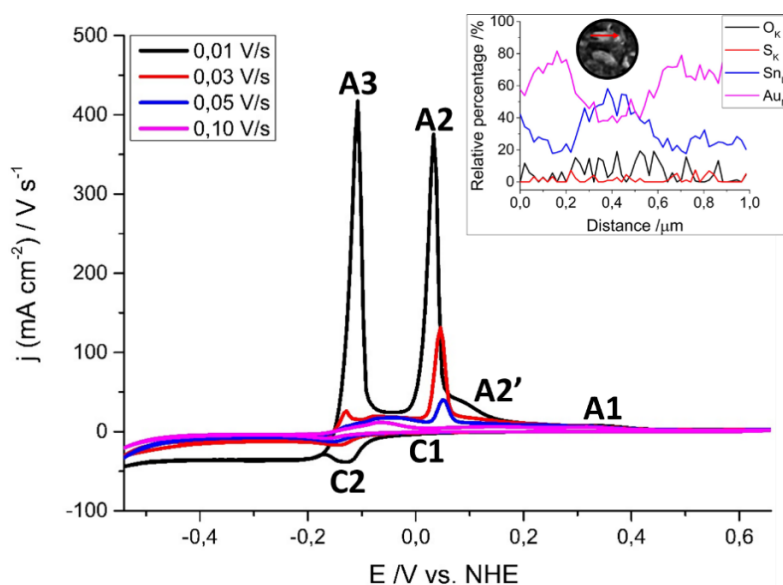


Fig B15. Cyclic voltammogram of tin electrodeposition on RDE polycrystalline gold, 0.1 M H₂SO₄, 200 μ M C₁₀H₇NaO₃S at different scan rates, 30 mV s⁻¹ and 1600 rpm. Inset shows the spectrum of the EDX microanalysis of a nanoparticle in the tin deposit.

B.7 Number of Sn ML on the gold substrate

Fig. B16 shows the linear sweep voltammetry and the transient recorded during the tin deposition in the absence and presence of naphthalene-based additives. Transients recorded in the absence and presence of NPTS and HNPTS exhibit almost identical current, with a small difference seen in the presence of NPT, due to a slight variation of the Sn (II) concentration in the solution. Furthermore, in the presence of ENSA, a strong decrease in the current is seen in agreement with the strong inhibition of tin deposition.

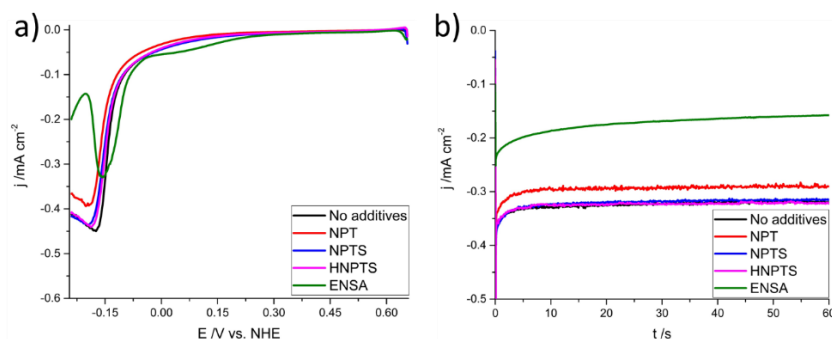


Fig B16. Linear sweep voltammetry and subsequent chronoamperometry of tin electrodeposition on RDE polycrystalline gold, 0.1 M H₂SO₄, 0.6 mM SnSO₄ in the absence and presence of 200 μ M of: NPT, NPTS HNPTS and ENSA at 1600 rpm.

B.8 Scanning electron micrographs of gold substrates

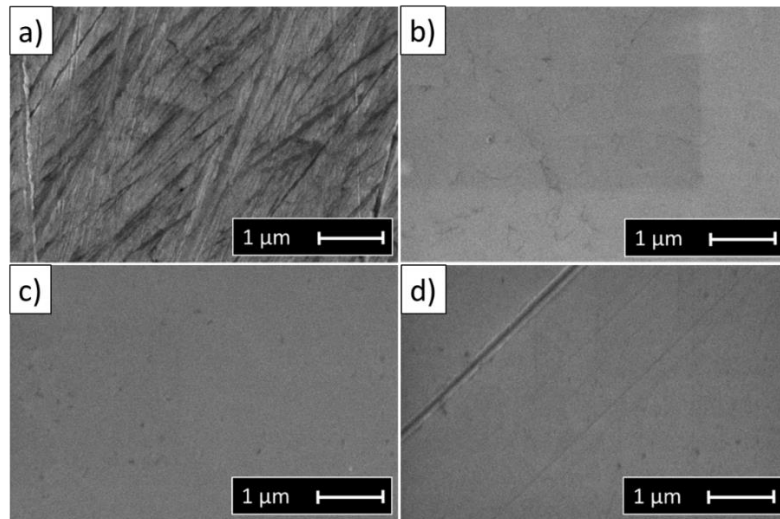


Fig B17. Scanning electron micrographs of: (a) polycrystalline gold (b) Au (100) (c) Au (110) (d) Au (111)

APPENDIX

C

Supporting information to Chapter 4:

The effect of naphthalene-based additives on the kinetics of tin electrodeposition on a boron doped diamond electrode

C.1 Effect of naphthalene-based additives on the tin (II) diffusion coefficient

Table C1 show the tin (II) diffusion coefficients in the absence and presence of different concentrations of NPT, NPTS and HNPTS. Values were calculated at high negative potential by fitting the current transient to the Cottrell equation.

Table C1. Tin (II) diffusion coefficient ($D_{Sn^{2+}}$) in the absence and presence of naphthalene-based additives at different concentrations, at -0.460 V.

Additive	Concentration / mM	$D_{Sn^{2+}} / cm^2 s^{-1}$
NPT	0	$7.7 \pm 0.2 \times 10^{-6}$
	0.1	8.0×10^{-6}
	0.5	6.8×10^{-6}
	1.0	6.8×10^{-6}
NPTS	0	$7.7 \pm 0.23 \times 10^{-6}$
	0.1	7.2×10^{-6}
	0.5	5.8×10^{-6}
	1.0	7.0×10^{-6}
HNPTS	0	$7.7 \pm 0.2 \times 10^{-6}$
	0.1	5.3×10^{-6}
	0.5	5.6×10^{-6}
	1.0	7.3×10^{-6}

Table C2 show the tin (II) diffusion coefficients in the absence and presence of different concentrations of NPT, NPTS and HNPTS. Values were calculated at lower negative potentials by fitting the current transient to the Cottrell equation.

Table C2. Diffusion coefficients ($D_{Sn^{2+}}$) in the absence and presence of naphthalene-based additives at different concentrations at different applied potentials.

-E /V	No additives $D_{Sn^{2+}} / cm^2 s^{-1}$	NPT (1 mM) $D_{Sn^{2+}} / cm^2 s^{-1}$	NPTS (1 mM) $D_{Sn^{2+}} / cm^2 s^{-1}$	HNPTS (1 mM) $D_{Sn^{2+}} / cm^2 s^{-1}$
-0.340	7.3×10^{-6}	7.8×10^{-6}	7.5×10^{-6}	6.4×10^{-6}
-0.365	7.8×10^{-6}	7.3×10^{-6}	7.8×10^{-6}	6.9×10^{-6}
-0.390	7.7×10^{-6}	6.5×10^{-6}	9.5×10^{-6}	7.3×10^{-6}
-0.415	7.4×10^{-6}	6.3×10^{-6}	9.5×10^{-6}	7.6×10^{-6}
-0.440	7.2×10^{-6}	7.0×10^{-6}	6.6×10^{-6}	6.5×10^{-6}

C.2 Effect of naphthalene-based additives on the nucleation mode of tin deposits on a boron doped diamond electrode

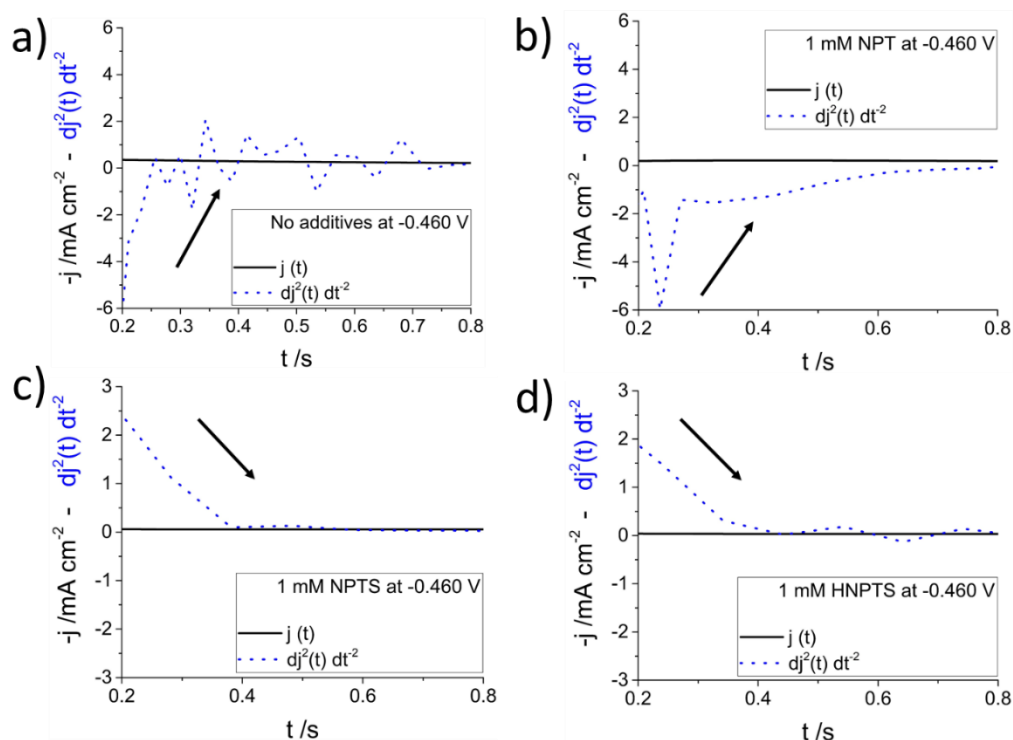


Figure C1. Current transient $j(t)$ and second derivative $\frac{d^2 j(t)}{dt^2}$ for current transients recorded in 0.1 M H_2SO_4 , 0.5 Mm SnSO_4 at -0.460 V in the (a) absence, and the presence of 1 mM (b) NPT, (c) NPTS, and (d) HNPTS

Current transients recorded at -0.460 V (the highest negative potential) in the absence of additives and presence of NPT, figures C1a and C1b respectively, exhibit a negative second derivative at short times, characteristic of instantaneous nucleation mode. The measurements in the presence of NPTS and HNPTS, fig C1c and C1d respectively show a positive second derivative, characteristic of progressive nucleation mode. Results show that NPT does not change the tin nucleation mode on BDD, in contrast to NPTS, and HNPTS that change the nucleation mode from instantaneous to progressive.

C.3 Effect of naphthalene-based additives on the morphology of tin deposits on a boron doped diamond electrode

Figure C2, C3, C4, C5 and C6 show the scanning electron micrographs of tin deposits on a boron doped diamond electrode grown in the absence and in the presence of NPT, NPTS, HNPTS and ENSA, respectively.

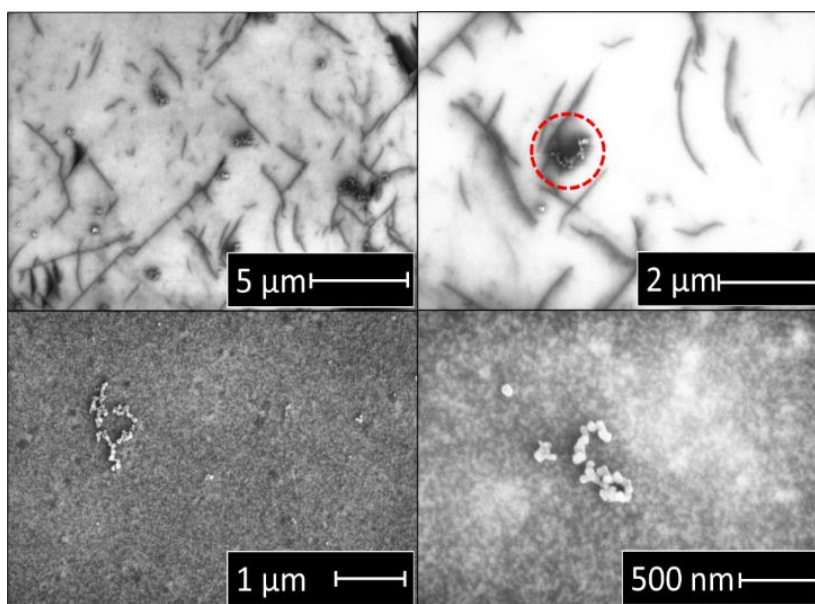


Figure C2. Scanning electron micrographs of tin electrodeposited on a boron doped diamond surface in 0.1 M H_2SO_4 and 0.5 mM SnSO_4 . Potential was held at -0.266 V for 10 s where nucleation and early growth happened, subsequently potential was held at -0.230 V during 60 s where the nuclei were grown.

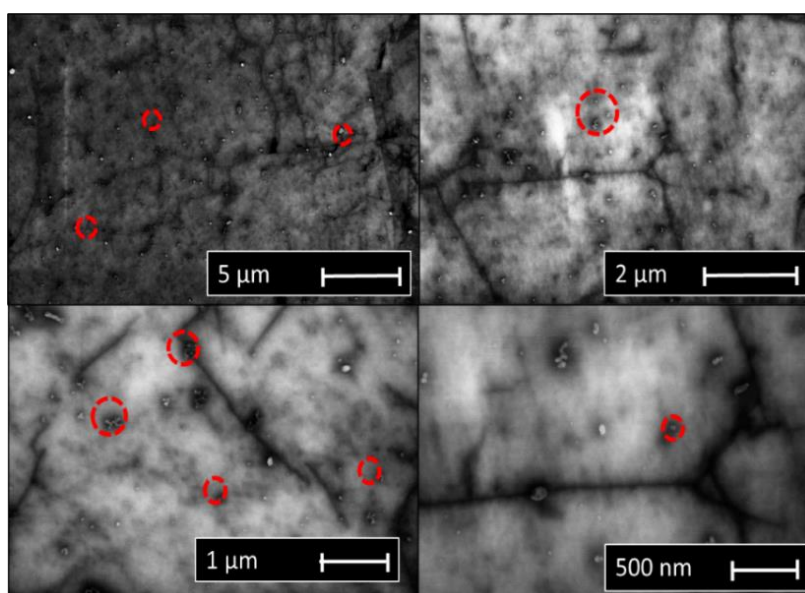


Figure C3. Scanning electron micrographs of tin electrodeposited on a boron doped diamond surface in 0.1 M H_2SO_4 and 0.5 mM SnSO_4 and in the presence 1 mM of NPT. Potential was held at -0.266 V for 10 s where nucleation and early growth happened, subsequently potential was held at -0.230 V during 60 s where the nuclei were grown.

C3. Effect of naphthalene-based additives on the morphology of tin deposits on BDD

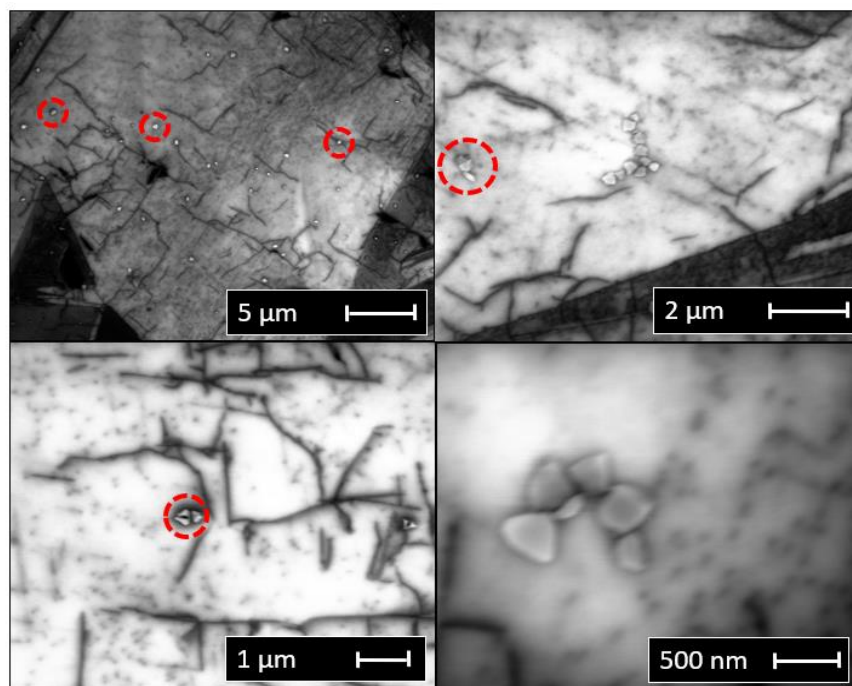


Figure C4. Scanning electron micrographs of tin electrodeposited on a boron doped diamond surface in 0.1 M H_2SO_4 and 0.5 mM SnSO_4 and in the presence 1 mM of NPTS. Potential was held at -0.266 V for 10 s where nucleation and early growth happened, subsequently potential was held at -0.230 V during 60 s where the nuclei were grown.

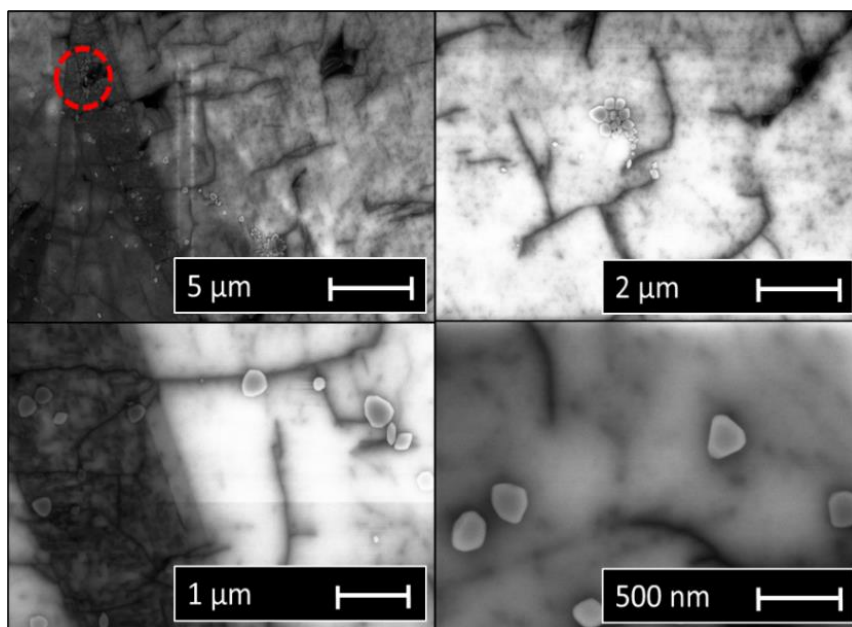


Figure C5. Scanning electron micrographs of tin electrodeposited on a boron doped diamond surface in 0.1 M H_2SO_4 and 0.5 mM SnSO_4 and in the presence 1 mM of HNPTS. Potential was held at -0.266 V for 10 s where nucleation and early growth happened, subsequently potential was held at -0.230 V during 60 s where the nuclei were grown.

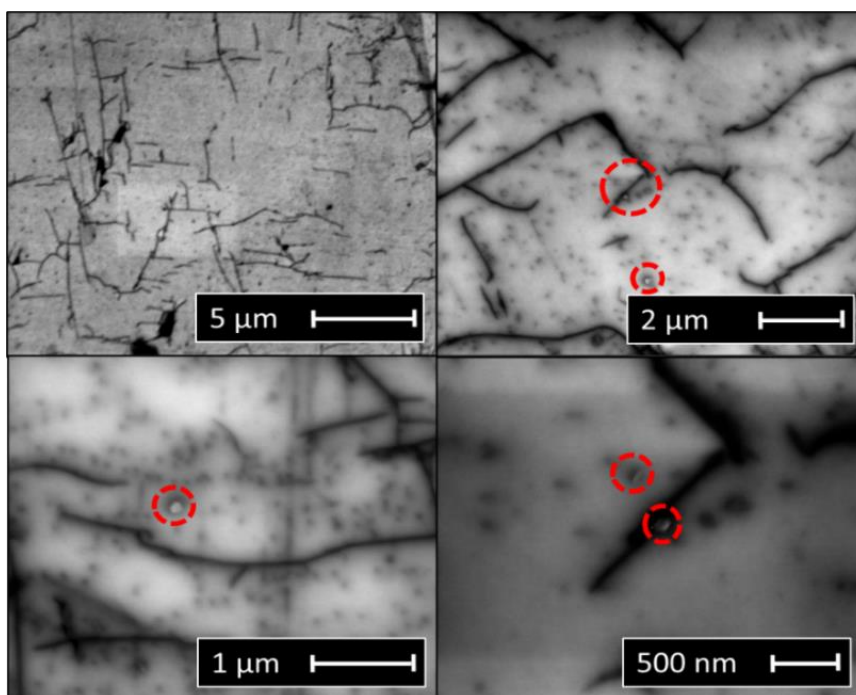


Figure C6. Scanning electron micrographs of tin electrodeposited on a boron doped diamond surface in 0.1 M H_2SO_4 and 0.5 mM SnSO_4 and in the presence 1 mM of ENSA. Potential was held at -0.266 V for 10 s where nucleation and early growth happened, subsequently potential was held at -0.230 V during 60 s where the nuclei were grown.